scientific reports

Check for updates

OPEN

Bandwidth and gain enhancement of composite right left handed metamaterial transmission line planar antenna employing a non foster impedance matching circuit board

Mohammad Alibakhshikenari[1]✉, Bal S. Virdee[2], Ayman A. Althuwayb[3], Leyre Azpilicueta[4], Naser Ojaroudi Parchin[5], Chan H. See[6], Raed A. Abd-Alhameed[5], Francisco Falcone[7,8], Isabelle Huynen[9], Tayeb A. Denidni[10] & Ernesto Limiti[1]

The paper demonstrates an effective technique to significantly enhance the bandwidth and radiation gain of an otherwise narrowband composite right/left-handed transmission-line (CRLH-TL) antenna using a non-Foster impedance matching circuit (NF-IMC) without affecting the antenna's stability. This is achieved by using the negative reactance of the NF-IMC to counteract the input capacitance of the antenna. Series capacitance of the CRLH-TL unit-cell is created by etching a dielectric spiral slot inside a rectangular microstrip patch that is grounded through a spiraled microstrip inductance. The overall size of the antenna, including the NF-IMC at its lowest operating frequency is $0.335\lambda_0 \times 0.137\lambda_0 \times 0.003\lambda_0$, where λ_0 is the free-space wavelength at 1.4 GHz. The performance of the antenna was verified through actual measurements. The stable bandwidth of the antenna for $|S_{11}| \leq -18$ dB is greater than 1 GHz (1.4–2.45 GHz), which is significantly wider than the CRLH-TL antenna without the proposed impedance matching circuit. In addition, with the proposed technique the measured radiation gain and efficiency of the antenna are increased on average by 3.2 dBi and 31.5% over the operating frequency band.

Highly reliable and portable ultra-high frequency (UHF) wireless communication systems mainly employ monopole or dipole antennas. As the physical size of the antenna is proportional its operating wavelength, UHF-band antennas can have a length between 0.1 to 1 m. Various types of small UHF-band antennas have been previously proposed; however, they cannot be adapted for conformal installations and/or their bandwidth is limited[1–3]. Another method to reduce the antenna size is using metamaterials (MTMs) or left-handed (LH) ($\varepsilon < 0, \mu < 0$) materials[4–6]. In practice, when creating a MTM the parasitic elements associated with transmission-lines (TLs), i.e. right-handed (RH) ($\varepsilon > 0, \mu > 0$), combine with the LH characteristics to create a MTM structure commonly referred to as composite right/left-handed transmission-line (CRLH-TL)[7]. Antennas based on CRLH-TLs can be designed to operate in different modes, such as the zeroth-order resonance (ZOR) mode, + 1, and − 1 modes[8,9].

[1]Electronic Engineering Department, University of Rome "Tor Vergata", Via Del Politecnico 1, 00133 Rome, Italy. [2]Center for Communications Technology, London Metropolitan University, London N7 8DB, UK. [3]Department of Electrical Engineering, Jouf University, Sakaka 72388, Aljouf, Saudi Arabia. [4]School of Engineering and Sciences, Tecnologico de Monterrey, 64849 Monterrey, Mexico. [5]Faculty of Engineering and Informatics, University of Bradford, Bradford BD7 1DP, West Yorkshire, UK. [6]School of Engineering and the Built Environment, Edinburgh Napier University, 10 Colinton Rd, Edinburgh EH10 5DT, UK. [7]Electronic and Communication Engineering Department, Public University of Navarre, 31006 Pamplona, Spain. [8]Institute of Smart Cities, Public University of Navarre, 31006 Pamplona, Spain. [9]Institute of Information and Communication Technologies, Electronics and Applied Mathematics, Université Catholique de Louvain, 1348 Louvain-la-Neuve, Belgium. [10]Institut National de La Recherche Scientifique (INRS), University of Quebec, Montréal, Québec H5A 1K6, Canada. ✉email: alibakhshikenari@ing.uniroma2.it

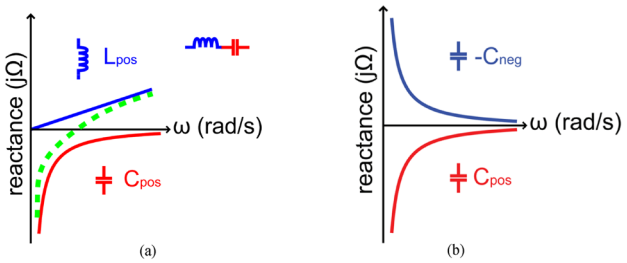

Figure 1. Matching with (**a**) Foster impedance, and (**b**) non-Foster impedance.

The zeroth-order resonance frequency makes CRLH-TLs independent of its physical dimensions. This property is taken advantage of here to miniaturize the antenna. As CRLH-TL can be easily realized using standard printed circuit board (PCB) technologies they have been used in the design of multiband antennas[10], frequency reconfigurable antennas[11] and pattern reconfigurable antennas[8]. However, the inherent narrow bandwidth of CRLH-TLs limits the range of applications of this type of antenna.

To overcome the bandwidth limitation of CRLH-TL antenna, it is necessary to introduce an active device that presents a negative reactance that counteracts the positive reactance of the antenna. This is achieved here with the use of a non-Foster impedance matching circuit. The challenging aspect of NF-IMC design is a stability-performance tradeoff, where instability leads to oscillation or latching. Optimal performance is achieved at the stability threshold, leaving little margin for error due to imperfect modeling, fabrication tolerances, and environmental changes. Numerous designs of the non-Foster circuit have been previously reported to realize wideband matching of electrically small antennas[12–15]. The improvement in the matching performance reported using NF-IMC is mainly in terms of reflection-coefficient, which does not completely characterize the antenna's operational band.

In this paper we demonstrate that by combining the proposed non-Foster impedance matching circuit (NF-IMC) with a narrowband CRLH-TL microstrip antenna it is possible to significantly enhance the antenna's bandwidth and radiation gain performance without compromising its stability. This is due to the negative reactance created by the NF-IMC that is used to cancel the antenna's high and positive reactance over its operating frequency range. The proposed antenna described here is implemented with six unit-cells of CRLH-TL, where the equivalent circuit of each unit-cell consists of series left-handed capacitance and shunt spiral left-handed inductance. The size of the proposed antenna is $56 \times 20 \times 0.8$ mm^3 or $0.261\ \lambda_0 \times 0.093\ \lambda_0 \times 0.003\ \lambda_0$, where λ_0 is at the minimum operation frequency of the antenna which is 1.4 GHz. The size of the non-Foster circuit is $0.074\ \lambda_0 \times 0.044\ \lambda_0$ (16×9.5 mm^2). The proposed antenna has a measured bandwidth of > 1 GHz across 1.4–2.45 GHz for $|S_{11}| \leq -18$ dB, which is significantly wider than the CRLH-TL antenna without the non-Foster circuitry. With NF-IMC the measured antenna's radiation gain is shown to improve over its operating frequency range on average by approximately 3 dB.

Design of non-foster impedance matching circuit

Impedance matching circuits (IMCs) using conventional passive elements such as a *LC*-circuit are applicable only for narrowband devices. To circumvent this issue the negative impedance property of NF-IMC is exploited here to reverse the reactance slope of conventional *LC*-circuits, as illustrated in Fig. 1, to thereby accomplish impedance matching over a wider band. The design of the NF-IMC is based on the generic principle described in[16] involving the use of cross-coupled transistors, as shown in Fig. 2a. This circuit is utilized here to convert the load impedance (Z_{ref}) seen by the two transistors to its negative equivalent. Positive feedback loop is created by cross coupling the gate and drain of the two transistors, which is typically used to design an oscillator circuit. Therefore, avoiding oscillations and ensuring stability are critical in the design of the NF-IMC. In the cross-coupled transistor arrangement the phase of the current at the input and output are identical, but there is a phase difference between the input and output voltages of 180°. From the small-signal model of the simplified NF-IMC topology in Fig. 2b, it can be shown that

$$Z_{in} = \frac{2r_o}{1 + g_m r_o} + \frac{Z_{ref}}{1 + g_m r_o} - \frac{Z_{ref} g_m r_o}{1 + g_m r_o} \tag{1}$$

where r_o and g_m are the transistor's output resistance and transconductance, respectively. Assuming $g_m r_o \gg 1$ and is large compared to Z_{ref}, (1) can be approximated as $Z_{in} = -Z_{ref}$. The actual NF-IMC used in Fig. 2c was obtained through optimization using ADS from Keysight Technologies to provide impedance matching from 1.4 to 2.45 GHz. The optimized parameters of the NF-IMC are given in Table 1. Avago ATF-53189 transistor with an operating frequency of 50–6500 MHz was used here. The bias voltage V_{DD} is 2 V.

Active feedback is necessary in NF-IMC to realize the desired negative impedance. However, NF-IMCs can generate positive feedback when connected to the antenna system which can adversely affect its stability. As NF-IMC's delicate stability is vulnerable to environmental changes, a small perturbation in antenna's impedance could increase the positive feedback and make the NF-IMCs deviate from the stable condition into a large signal oscillator. It was therefore important to establish the stability of the NF-IMC. Stability over a wide band was achieved by cross coupling the transistors with series *LC* circuit. The stability was confirmed by checking

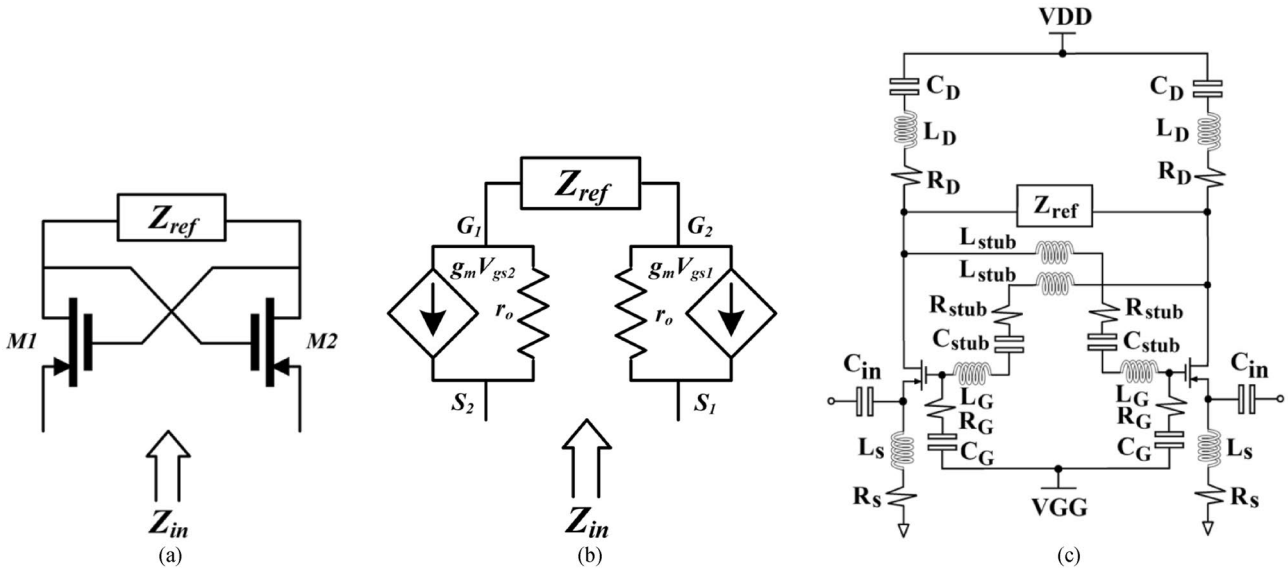

Figure 2. Non-Foster impedance matching circuit (NF-IMC) obtained through optimization using ADS version 2019 from Keysight Technologies. (**a**) Basic topology, (**b**) equivalent small-signal model, and (**c**) equivalent circuit of the optimized NF-IMC design used here.

Parameter	Value
Z_{ref}	13 pF
C_D	125 pF
L_D	150 nH
R_D	700 Ω
C_{stub}	8.5 pF
R_{stub}	50 Ω
L_{stub}	12 nH
C_{in}	50 pF
L_S	150 nH
R_S	700 Ω
C_G	125 pF
L_G	150 nH
R_G	700 Ω

Table 1. Parameters of the non-Foster impedance matching circuit (NF-IMC).

impedance of the NF-IMC and the time domain transient response, as shown in Fig. 3. The stability was maintained by making the impedance of the non-Foster matching circuit smaller than the impedance of the antenna, which is confirmed in Fig. 3a over 1.4–2.45 GHz. Figure 3b shows the time domain transient response of the NF-IMC is stable after 0.2 microseconds of switching 'on' the NF-IMC.

Design of proposed CRLH-TL antenna

The equivalent circuit of a typical CRLH-TL unit-cell is constituted from a left-handed (LH) and right-handed (RH) circuitry[7], where the LH circuit is composed of the series capacitors (C_L) and the shunt inductors (L_L). In practice, the unavoidable parasitic reactance elements are introduced in transmission-line structure, in particular series RH inductances (L_R) and the parasitic shunt RH capacitances (C_R) which compromise the existence of the purely LH circuit. The zeroth-order resonant frequency of the CRLH-TL is affected by these parasitic effects. Below the zeroth-order resonant frequency, CRLH-TL structure exhibits LH characteristics, and above zeroth-order resonant frequency, CRLH-TL exhibits RH characteristics. At the zeroth-order frequency, the resonant frequency is independent of the physical size. This property is exploited here to miniaturize the antenna. The zeroth-order resonant frequency is controlled by the series and shunt resonant frequencies defined by

$$\omega_{se} = 1/\sqrt{L_R C_L} \tag{2}$$

$$\omega_{sh} = 1/\sqrt{L_L C_R} \tag{3}$$

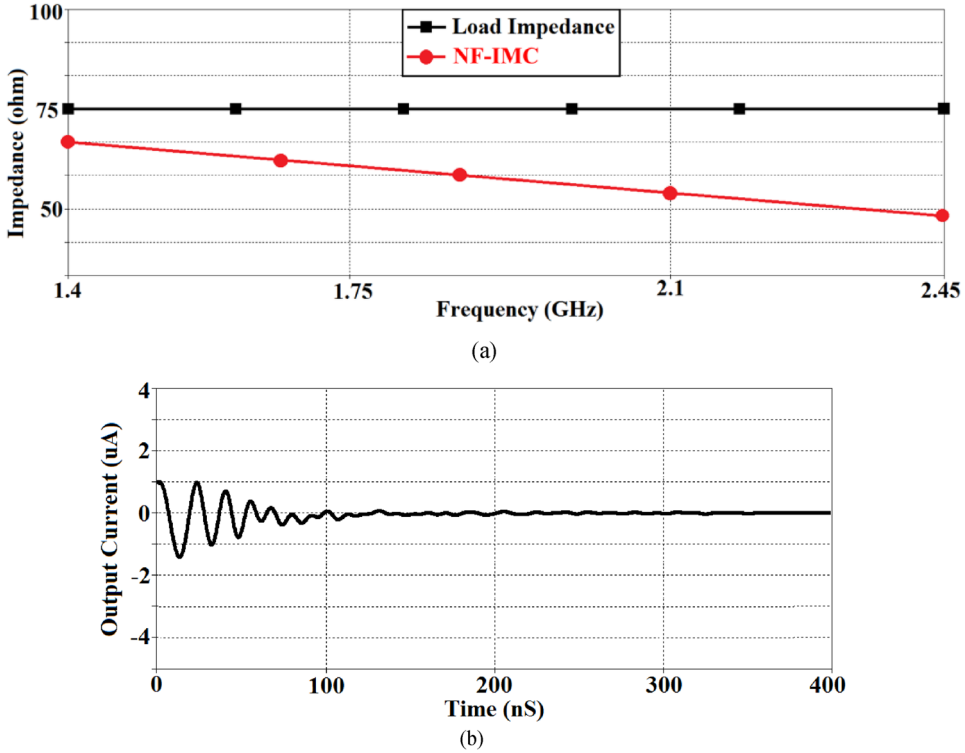

Figure 3. (**a**) Impedance of the proposed non-Foster matching circuit and load impedance (Z_{ref}), and (**b**) time domain transient response of the NF-IMC.

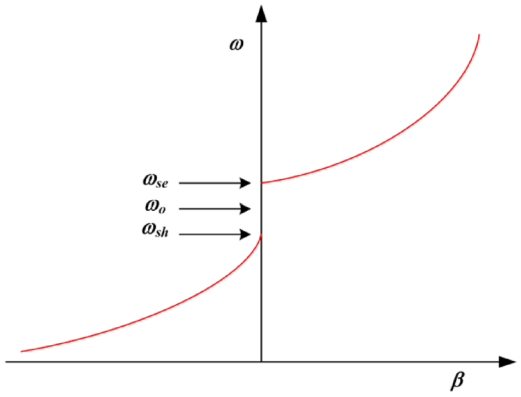

Figure 4. Dispersion curve of CRLH-TL unit-cell.

The propagation constant (β) for a CRLH unit-cell is given by

$$\beta = S(\omega)\sqrt{\omega^2 L_R C_R + \frac{1}{\omega^2 L_L C_L} - \left(\frac{L_R}{L_L} + \frac{C_R}{C_L}\right)} \tag{4}$$

where

$$S(\omega) = \begin{cases} -1 \text{ if } \omega < \omega_{\text{sh}} = min\left(\frac{1}{\sqrt{L_R C_L}}, \frac{1}{\sqrt{L_L C_R}}\right) \\ +1 \text{ if } \omega < \omega_{\text{se}} = max\left(\frac{1}{\sqrt{L_R C_L}}, \frac{1}{\sqrt{L_L C_R}}\right) \end{cases} \tag{5}$$

Figure 4 shows the dispersion diagram of a typical CRLH-TL unit-cell when ω_{se} and ω_{sh} are unequal. At these resonant frequencies (ω_{se} and ω_{sh}) where $\beta = 0$, an infinite wavelength can be supported. According to the transmission-line theory CRLH-TL resonates at a frequency given by [7]

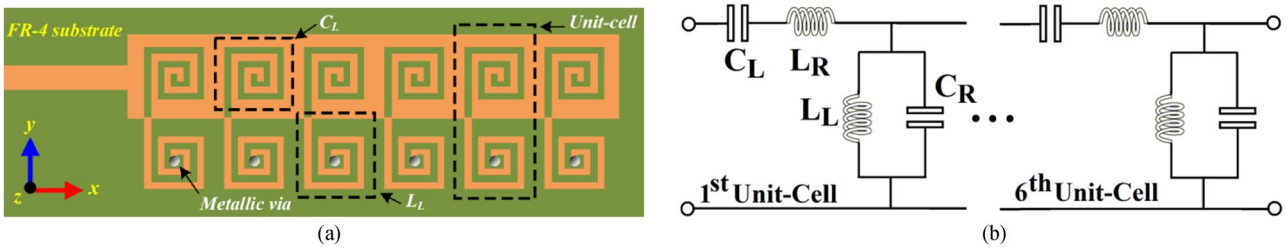

Figure 5. The proposed CRLH-TL antenna, (**a**) layout, realized in CST Microwave Studio version 2019, and (**b**) equivalent circuit, obtained through optimization using ADS version 2019.

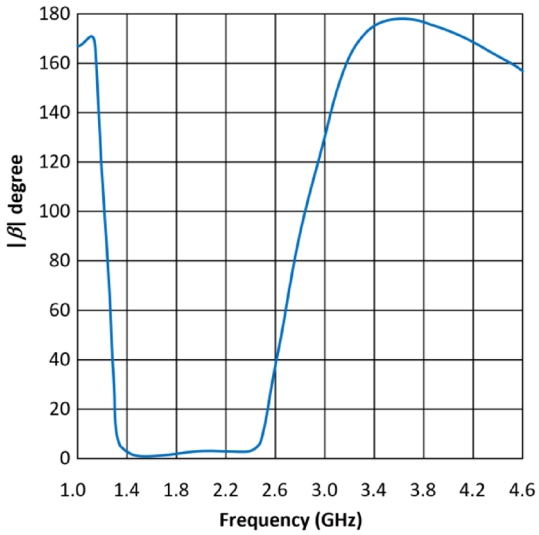

Figure 6. Dispersion diagram of the proposed CRLH-TL unit-cell.

$$\beta_n = \frac{n\pi}{l}(n = 0, \pm 1, \pm 2, \ldots, \pm(N-1)) \tag{6}$$

where, l, n and N are the physical length of the resonator, mode number, and number of unit cells, respectively. When n is zero, the wavelength, $\lambda_g = 2\pi/|\beta_n|$, becomes infinite and the resonant frequency of the zeroth-order mode becomes independent of the size of the resonator.

The antenna was designed by determining the reactance values in Eqs. (2) & (3) such that each of the two zeroth-order resonant frequencies define the boundary of the frequency range of interest. This was done by using the optimization tool in ADS by Keysight Technologies. The CRLH-TL unit-cell parameters were then converted to their physical implementation on microstrip technology, where C_L is implemented by etching a spiral slot on a rectangular patch, and the L_L is realized using a high impedance spiraled microstrip-line that is grounded with a metalized via-hole. The inductor was spiraled purely to minimize the spaced used. As mentioned earlier the parasitic RH elements (C_R & L_R) are unavoidable components in the transmission-line structure due to existence of the voltage gradient between the patch and ground plane, and the currents flowing on the surfaces, respectively[13]. As these parameters effect the overall frequency range of the antenna it was therefore necessary to optimize the structural parameters of the antenna unit-cell using ADS to realize the desired performance. The physical layout of the proposed antenna, which consists of a cascade of six unit-cells, and its equivalent circuit are shown in Fig. 5. The dispersion diagram of the CRLH-TL unit-cell depicted in Fig. 6 shows the LH and RH regions are 1.14 GHz $< f_{LH} <$ 1.41 GHz and 2.45 GHz $< f_{RH} <$ 3.6 GHz, respectively. It also shows the propagation constant of the CRLH-TL unit-cell is near zero in the frequency range of interest between 1.4 and 2.46 GHz. The simulation analysis in Fig. 7 reveals show the input impedance of the antenna is affected by the number of unit-cells. The antenna was implement using six unit-cells so that its impedance was compatible with the 50Ω NF-IMC board.

The proposed CRLH-TL antenna was constructed on the FR-4 lossy substrate with ε_r=4.4, thickness h = 0.8 mm, and tan δ=0.025. The equivalent circuit parameters of the CRLH-TL unit-cell were extracted using the pseudo-inverse method[17] from the measured S-parameters. This involved converting the S-parameters to $ABCD$-parameters and the corresponding impedance and admittance from which the values of the lumped elements were obtained. The averaged values of the unit-cell parameters over the frequency of interest (1.4–2.45 GHz) are: $L_L = 0.39nH$, $C_L = 6.12pF$, $L_R = 2.11nH$, and $C_R = 10.74pF$. The structural parameters of the optimized antenna are given in Table 2, where λ_0 is the free-space wavelength at 1.4 GHz.

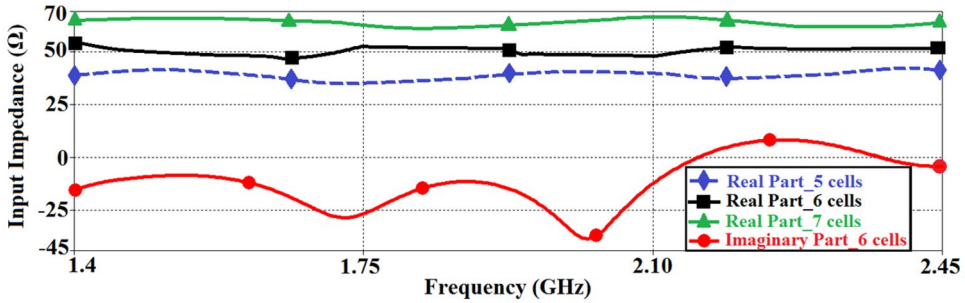

Figure 7. Input impedance of the CRLH-TL antenna as a function of number of unit-cells.

Number of spiral slot turns	3
Width of spiral slots	0.75 mm
Gap between spiral slots	0.75 mm
Gap between the unit-cells	2.25 mm
Number of inductive spiral turns	3
Width of inductive spiral	0.75 mm
Gap between the inductive spirals	0.75 mm
Radius of the via-hole	0.4 mm
Number of unit-cells	6
Unit-cell dimensions	$7 \times 16 \times 0.8$ mm^3 ($0.032\,\lambda_0 \times 0.074\,\lambda_0 \times 0.003\,\lambda_0$)
Antenna dimensions	$56 \times 20 \times 0.8$ mm^3 ($0.261\,\lambda_0 \times 0.093\,\lambda_0 \times 0.003\,\lambda_0$)
Ground-plane dimensions	$56 \times 20 \times 0.035$ mm^3
Dimensions of feedline	13×2.3 mm^2
Dimensions of NF-IMC board	16×9.5 mm^2

Table 2. Structural Parameters of the CRLH-TL Antenna.

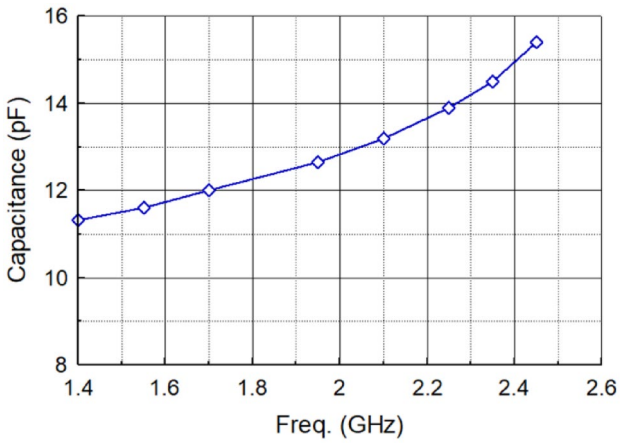

Figure 8. Input capacitance of the antenna as a function of frequency.

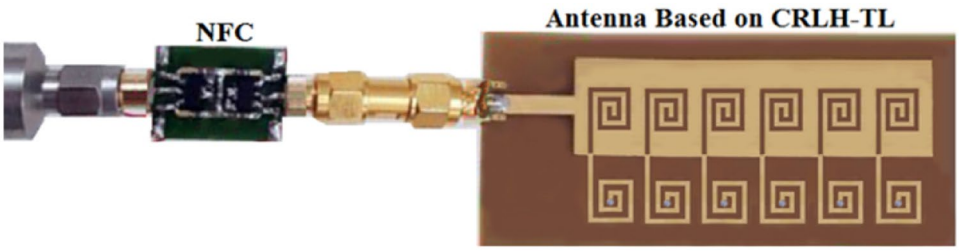

Figure 9. Fabricated CRLH-TL antenna prototype connected to NF-IMC board.

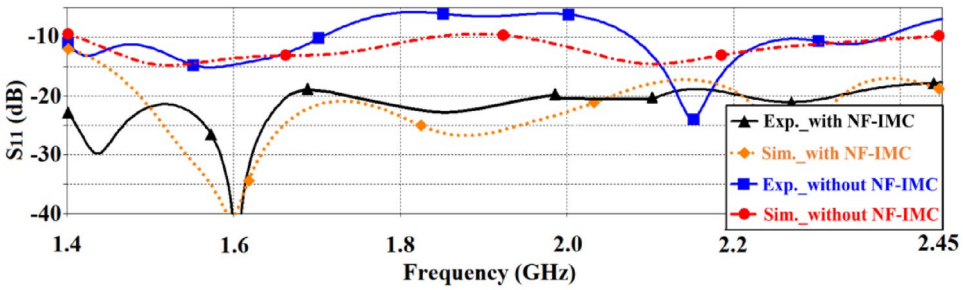

Figure 10. Simulated and measured reflection-coefficient response of the proposed CRLH-TL antenna without and with NF-IMC.

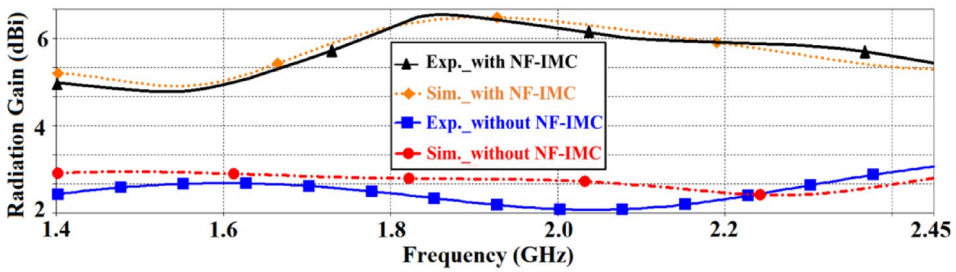

(a)

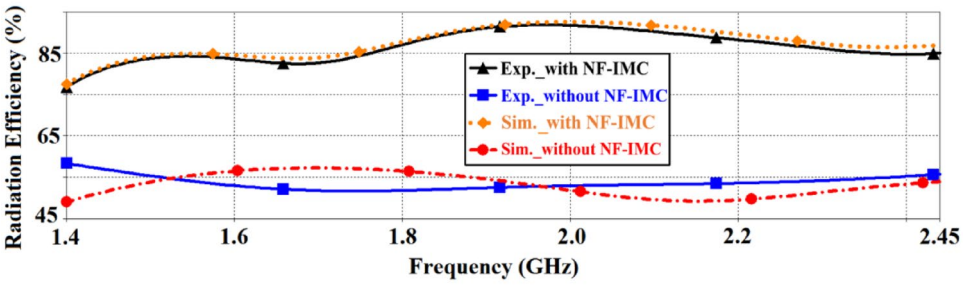

(b)

Figure 11. Simulated and measured radiation properties of the proposed CRLH-TL antenna with and without NF-IMC in the *xy*-plane, (**a**) gain, and (**b**) efficiency.

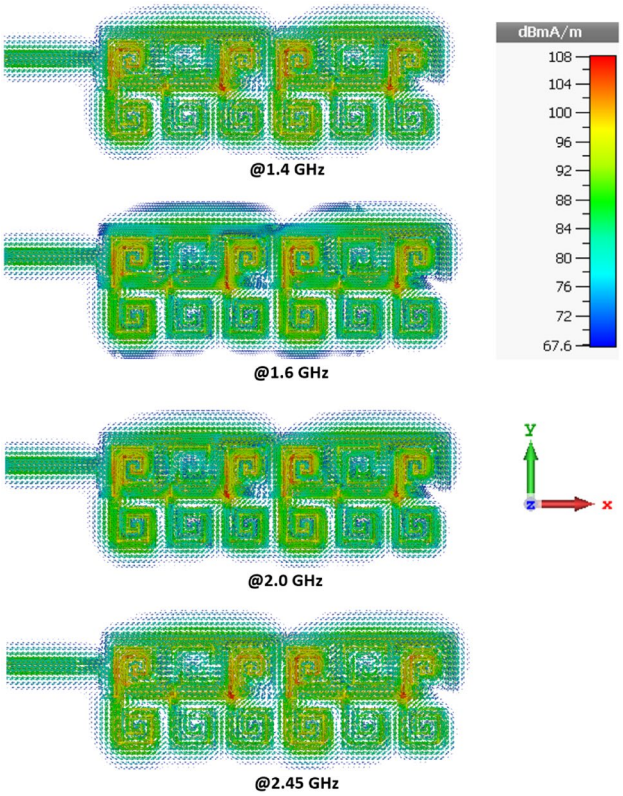

Figure 12. Current density distributions over the proposed antenna at spot frequencies of 1.4 GHz, 1.6 GHz, 2.0 GHz, and 2.45 GHz.

The input capacitance of the antenna is approximated by $Imag(Z_{in}) = 1/j\omega C$. The antenna's input capacitance as a function of frequency is shown in Fig. 8. The input capacitance of the antenna was counteracted with the negative reactance generated by the NF-IMC and thereby overcome the inherent narrowband characteristic of the antenna.

Fabricated prototype and measurements

The fabricated prototype of the proposed antenna based on CRLH-TL is combined with the NF-IMC as shown in Fig. 9. An SMA male to SMA male coupler is used to connect the antenna to NF-IMC board. With the antenna connected to the NF-IMC board the measured reflection-coefficient is better than − 18 dB across 1.4–2.45 GHz, which corresponds to a fractional bandwidth of 54.54%. Simulated and measured reflection-coefficient responses of the proposed antenna before and after applying NF-IMC are shown in Fig. 10. Although there is reasonably good correlation between the simulated and measured results the large disparity between 1.4 to 1.5 GHz is attributed to the manufacturing tolerances and unaccounted mismatch with the SMA male to SMA male coupler.

The simulated and measured radiation gain and efficiency in the *xy*-plane (E-plane) of the proposed antenna before and after applying NF-IMC are shown in Fig. 11. There is good correlation between the simulated and measured results. It is evident from these results that with NF-IMC the measured radiation gain increases by 3.2 dBi from an average of 2.4 dBi to 5.6 dBi across 1.4–2.45 GHz. Over the same frequency span the measured radiation efficiency of the antenna increased by 31.5% from an average of 54.5% to 86%.

Figure 12 shows how the current density is distributed over the surface of the antenna at various frequencies in its operating frequency band. It reveals the magnitude of the current is strongest over the middle two and outer unit-cells. The measured 2D radiation patterns of the antenna in the *xy*-plane (E-plane) and *xz*-plane (H-plane) with and without NF-IMC at 1.4 GHz and 2.45 GHz are shown in Fig. 13. The antenna's radiation energy is mainly focused in the *x*-direction. The beamwidth is much narrower in the *xy*-plane (E-plane).

The performance of the proposed CRLH-TL antenna with NF-IMC is compared with other state-of-the-art antennas reported in literature. The results of this study are summarized in Table 3. The main advantages of the proposed work are its simplicity and stability over a very wide (> 1 GHz) operating frequency range.

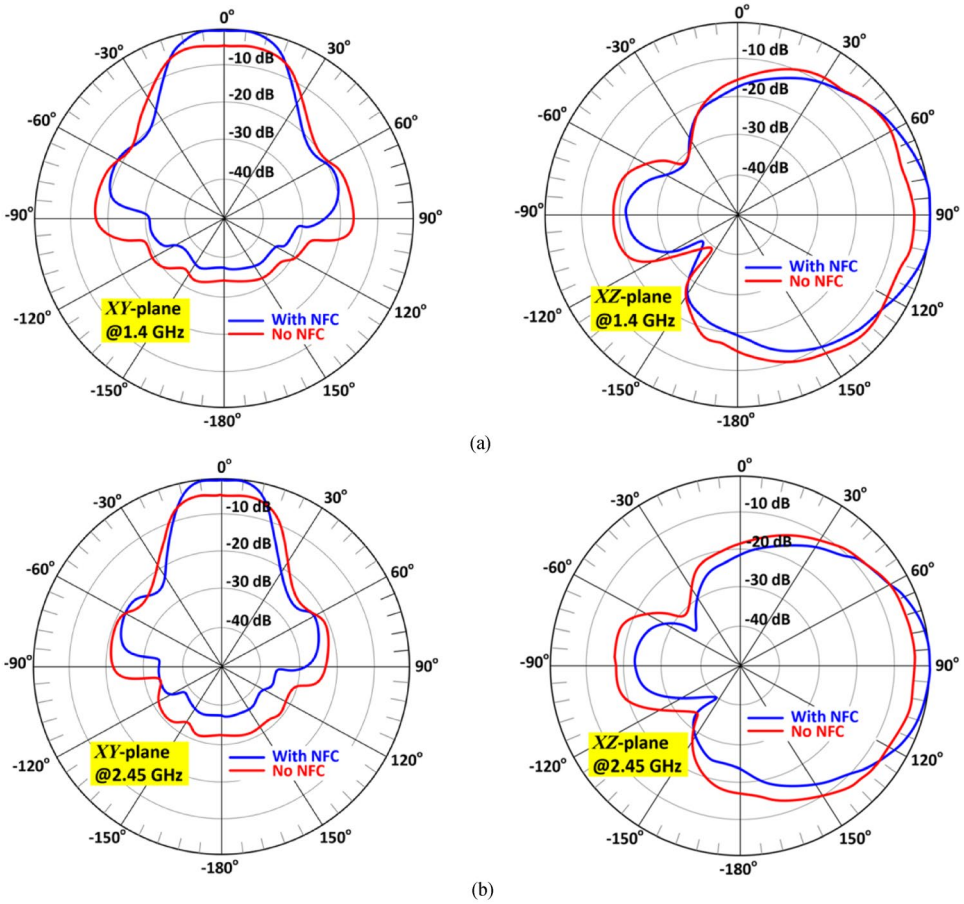

Figure 13. Measured radiation patterns (normalized) of the antenna without and with NF-IMC in the *xy*-plane (E-plane) and *xz*-plane (H-plane) at (**a**) 1.4 GHz and (**b**) 2.45 GHz.

References	FBW (%) [Freq. range]	Measured Gain (dBi)	Size (mm^3)	NF-IMC topology
[18]	4.9 [400-420 MHz]	1.05	Not given	Relatively simple
[19]	25.6 [85–110 MHz]	3	73 × 50 × 1.6	Relatively simple
[20]	66.7 [80–160 MHz]	3	20 × 20 × 0.5	Requires 4 transistors
[21]	3.6 [1.35–1.45 GHz]	Not given	70 × 48 × 0.5	Requires transversal filter using distributed amplifiers & delay lines
[22]	20 [1.0–1.5 GHz]	5	12 × 12 × 1	Requires four transistors
[23]	26.1 [100–130 MHz]	Not given	Not given	Relatively simple
This work	54.5 [1.4–2.45 GHz]	6.55	56 × 20 × 0.8	Relatively simple

Table 3. Performance Comparison Between the Proposed Work and Prior Arts.

Conclusions

It has been shown that by incorporating a non-Foster impedance matching circuit (NF-IMC) in-line with a miniature antenna, which is based on composite right/left-handed transmission-line technology, the operating bandwidth and radiation gain of the antenna can be substantially enhanced without affecting the antenna's stability. This is because the negative reactance generated by the NF-IMC is used to counteract the input capacitance of the antenna. The results presented demonstrate the effectiveness of this technique where the antenna's bandwidth is shown to increase from 380 MHz to greater than 1 GHz. Moreover, by incorporating the NF-IMC the average radiation gain and efficiency are shown to improve by 3.2 dBi and 31.5% over its operating bandwidth.

Received: 4 November 2020; Accepted: 22 March 2021
Published online: 02 April 2021

References

1. Nandi, S. & Mohan, A. CRLH unit cell loaded quad-band monopole antenna. *Microwave Opt. Tech. Lett.* **58**(3), 653–658 (2016).
2. Kim, S. & Lee, J. Frequency and bandwidth of the negative/positive nth mode of a composite right-/left-handed transmission line. *J. Electromagn. Eng. Sci.* **18**, 1–6 (2018).
3. Nelaturi, S. & Sarma, N. A compact microstrip patch antenna based on metamaterials for WiFi and WiMAX application. *J. Electromagn. Eng. Sci.* **18**, 182–187 (2018).
4. Yuan, Y. *et al.* Independent phase modulation for quadruplex polarization channels enabled by chirality-assisted geometric-phase metasurfaces. *Nat. Commun.* **11**, 4186. https://doi.org/10.1038/s41467-020-17773-6 (2020).
5. Zhang, K. *et al.* Polarization-engineered non interleaved metasurface for integer and fractional orbital angular momentum multiplexing. *Laser Photon. Rev.* https://doi.org/10.1002/lpor.202000351 (2021).
6. Yuan, Y. *et al.* A fully phase-modulated metasurface as an energy-controllable circular polarization router. *Adv. Sci.* **7**(18), 2001437. https://doi.org/10.1002/advs.202001437 (2020).
7. Caloz, C. & Itoh, T. *Electromagnetic Metamaterials: Transmission Line Theory and Microwave Applications* (Wiley-IEEE Press, 2005).
8. Zhang, J., Yan, S. & Vandenbosch, G. A. E. Realization of dual-band pattern diversity with a CRLH-TL-inspired reconfigurable metamaterial. *IEEE Trans. Antennas Propag.* **66**(10), 5130–5138 (2018).
9. Lee, H., Ren, D. & Choi, J. H. Dual-band and polarization-flexible CRLH substrate-integrated waveguide resonant antenna. *IEEE Antennas Wireless Propag. Lett.* **17**(8), 1469–1472 (2018).
10. Gupta, A. & Chaudhary, R. K. 'A miniaturized dual-band ZOR antenna using epsilon negative transmission line loading'. *Int. J. Microw. Wireless Technol.* **9**(8), 1735–1739 (2017).
11. Khan, M. S. *et al.* A frequency-reconfigurable series-fed microstrip patch array with interconnecting CRLH transmission lines. *IEEE Antennas Wireless Propag. Letters* **15**, 242–245 (2016).
12. Shih, T.-Y. & Behdad, N. Wideband, non-Foster impedance matching of electrically small transmitting antennas. *IEEE Trans. Antennas Propag.* **66**(11), 5687–5697 (2018).
13. Kim, T.-H., Yun, G.-H., Lee, W. & Yook, J.-G. Highly efficient WPT system with negative impedance converter for Q-factor improvement. *IEEE Access* **7**, 108750–108760 (2019).
14. White, C. R., Colburn, J. S. & Nagele, R. G. A non-Foster VHF monopole antenna. *IEEE Antennas Wirel. Propag. Lett.* **11**, 584–587. https://doi.org/10.1109/LAWP.2012.2201129 (2012).
15. Go, J.-G. & Chung, J.-Y. Non-Foster matching circuit design to improve VHF and UHF-band small antenna impedance matching. *J. Korean Inst. Electromagn. Eng. Sci.* **29**, 159–166 (2018).
16. Linvill, J. G. Transistor negative impedance converters. *Proc. IRE* **41**(6), 725–729 (1953).
17. Kou, N., Shi, Y. & Li, L. New equivalent circuit analysis and synthesis for broadband composite right/left-handed transmission line metamaterials. *ACES J.* **31**, 884–893 (2016).
18. Shi, T., Tang, M.-C., Wu, Z., Xu, H.-X. & Ziolkowski, R. W. Improved signal-to-noise ratio, bandwidth-enhanced electrically small antenna augmented with internal non-foster elements. *IEEE Trans. Antennas Propag.* **67**(4), 2763–2768 (2019).
19. Shen, Y. & Chio, T. Matching electrically small antenna using non-Foster circuit in the FM-band. *The 8th Europ. Conf. on Ant. & Propag. (EuCAP 2014)*, The Hague, 2014, pp. 333–336.
20. Albarracín-Vargas, F. *et al.* Design method for actively matched antennas with non-Foster elements. *IEEE Trans. Ant. Propag.* **64**(9), 4118–4123 (2016).
21. Zhang, T. *et al.* Unconditionally stable non-foster element using active transversal-filter-based negative group delay circuit. *IEEE Microw. Wirel. Comp. Lett.* **27**(10), 921–923 (2017).
22. Batel, L., Pintos, J. & Rudant, L. Superdirective and broadband compact antenna array using non-Foster elements. *Int. Workshop on Antenna Technology (iWAT)*, Miami, FL, USA, 2019, pp.17–20.
23. Jacob, M. M. *et al.* Non-Foster matched antennas for high-power applications. *IEEE Trans. On Ant. Propag.* **65**(9), 4461–4469 (2017).

Acknowledgements

This work is partially supported by RTI2018-095499-B-C31, Funded by Ministerio de Ciencia, Innovación y Universidades, Gobierno de España (MCIU/AEI/FEDER,UE), and innovation programme under grant agreement H2020-MSCA-ITN-2016 SECRET-722424 and the financial support from the UK Engineering and Physical Sciences Research Council (EPSRC) under grant EP/E022936/1.

Author contributions

Conceptualization, M.A., B.S.V., C.H.S., R.A.A.-A., F.F., I.H., T.A.D., and E.L.; methodology, M.A., B.S.V., F.F., I.H., T.A.D., and E.L.; software, M.A., B.S.V., and C.H.S.; validation, M.A., B.S.V., A.A.A., L.A., N.O.P., C.H.S., R.A.A.-A., F.F., I.H., T.A.D., and E.L.; formal analysis, M.A., B.S.V., C.H.S., R.A.A.-A., F.F., I.H., T.A.D., and E.L.; investigation, M.A., B.S.V., C.H.S., R.A.A.-A., F.F., I.H., T.A.D., and E.L.; resources, M.A., B.S.V., C.H.S., R.A.A.-A., F.F., I.H., T.A.D., and E.L.; data curation, M.A., B.S.V., A.A.A., L.A., N.O.P., C.H.S., R.A.A.-A., F.F., I.H., T.A.D., and E.L.; writing—original draft preparation, M.A.; writing—review and editing, M.A., B.S.V., A.A.A., L.A., N.O.P., C.H.S., R.A.A.-A., F.F., I.H., T.A.D., and E.L.; visualization, M.A., B.S.V., C.H.S., R.A.A.-A., F.F., I.H., T.A.D., and E.L.; supervision, E.L.; project administration, R.A.A.-A., F.F., and E.L.; funding acquisition, R.A.A.-A., F.F, E.L.

Competing interests

The authors declare no competing interests.

Additional information

Correspondence and requests for materials should be addressed to M.A.

Reprints and permissions information is available at www.nature.com/reprints.

Publisher's note Springer Nature remains neutral with regard to jurisdictional claims in published maps and institutional affiliations.

Open Access This article is licensed under a Creative Commons Attribution 4.0 International License, which permits use, sharing, adaptation, distribution and reproduction in any medium or format, as long as you give appropriate credit to the original author(s) and the source, provide a link to the Creative Commons licence, and indicate if changes were made. The images or other third party material in this article are included in the article's Creative Commons licence, unless indicated otherwise in a credit line to the material. If material is not included in the article's Creative Commons licence and your intended use is not permitted by statutory regulation or exceeds the permitted use, you will need to obtain permission directly from the copyright holder. To view a copy of this licence, visit http://creativecommons.org/licenses/by/4.0/.

© The Author(s) 2021